ACS Sustainable Chemistry & Engineering

Research Article

pubs.acs.org/journal/ascecg

Preparation of Nitrogen-Doped Carbon Spheres by Injecting Pyrolysis of Pyridine

Bin Cao, Huan Liu, Zhou Xing, Yaofei Lei, Huaihe Song,* Xiaohong Chen, Jisheng Zhou, and Zhaokun Ma

State Key Laboratory of Chemical Resource Engineering, Beijing Key Laboratory of Electrochemical Process and Technology for Materials, Beijing University of Chemical Technology, Beijing 100029, China

ABSTRACT: Nitrogen-doped carbon spheres (NDCS) with average diameter of 1.05 to 2.68 μm were synthesized by a simple and eco-friendly injecting pyrolysis using pyridine as the carbon precursor. The results indicated that both the pyrolysis temperature and injecting rate play important roles in controlling the morphology of NDCS. Because of the microstructure of concentric incompletely closed graphitic shells improving the thermal stability of nitrogen functionalities, the evolution of nitrogen functionalities in NDCS was much different from other nitrogen-doped carbon materials. The formation mechanism of NDCS was discussed and deduced. When NDCS were utilized as the anode material for lithium-ion batteries, they show high-rate performance and good cyclability, suggesting the advantages of injecting pyrolysis for large-scale generating anode material in power Li-ion batteries.

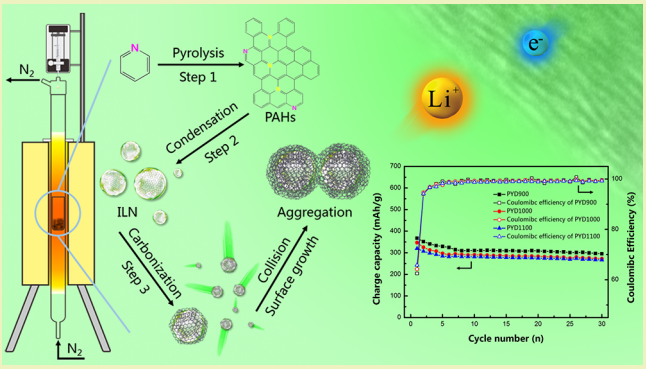

KEYWORDS: *Carbon spheres, Anode, Li-ion battery, Injecting pyrolysis, Nitrogen functionalities*

INTRODUCTION

The combination of sp, sp^2, sp^3 hybridization results in carbon materials' diverse range of structures and morphologies with extensive technical applications.[1] The discoveries of fullerenes,[2] carbon nanotubes[3] and graphene[4] have developed carbonaceous materials greatly in nanoscience and nanotechnology.[5−8] With the various structures and textures,[9] carbon materials have been used in many applications, such as energy storage, catalyst carrier, nanodevices, high strength composites and lubricants. Because of over-reliance on fossil fuels and the need for a better living environment, electrical energy has led to increased attention,[6,10,11] as it could be regenerated by renewable and sustainable technologies, including solar, wind and hydroelectric power. At the same time, high oil prices have pushed consumers toward electric or hybrid electric vehicles, which are critically dependent on the batteries. To improve environmental pollution and realize the goal of sustainable development, power Li-ion batteries are becoming a major technology for electric vehicles.[11,12] Therefore, carbon materials for energy storage have widely been investigated and will continue to have an enormous influence on our life.[13−18]

Carbon spheres can be synthesized by various methods, such as chemical vapor deposition (CVD),[1,19−24] pyrolysis,[25,26] spray pyrolysis,[27,28] hydrothermal treatment[29−31] and reactions under autogenic pressure at elevated temperature,[32,33] but few convenient methods have been proposed. Carbon spheres prepared by different methods usually have different microstructures that have direct influences on their electrochemical properties. Inagaki proposed a classification of spherical carbon structures according to their nanometric texture: concentric, radial or random arrangement of the carbon layers.[34] Compared with mesocarbon microbeads (MCMB) and graphite, carbon spheres with a microstructure of concentric incompletely closed graphitic shells usually have a low Li^+ storage capacity,[35] which may be due to the concentric microstructure providing less edge plan sites for intercalation and deintercalation of Li^+ ions. But this concentric microstructure is beneficial for long cycling life. Carbon spheres with concentric microstructure usually are prepared by traditional CVD, which has shortcomings of long preparation period, incomplete carbonization of precursor and difficulty for large-scale production. For the purposes of improving production efficiency, we use an injecting pyrolysis method to prepare directly carbon spheres efficiently. Compared with the traditional CVD method,[20] injecting pyrolysis has characteristics of short preparation period, high production efficiency and simple operation. Essentially, this method is a modified CVD due to their same gaseous phase carbonization mechanism. To the best of our knowledge, no one has yet explained the formation mechanism of carbon spheres prepared by the CVD method. According to serial experiment results,

Received: April 27, 2015
Revised: June 17, 2015
Published: June 24, 2015

DOI: 10.1021/acssuschemeng.5b00359
ACS Sustainable Chem. Eng. 2015, 3, 1786−1793

this paper explores the formation mechanism of carbon spheres during gaseous phase carbonization.

Carbon spheres have been proved to be a competent as an anode material for Li-ion batteries owing to their high packing density, low surface-to-volume ratio and maximal structural stability, etc.[30] Because high rate performance of anode materials for Li-ion batteries is strongly dependent on the size of particles,[36] reducing the size of carbon spheres is an effective way. To utilize the stable concentric microstructure of carbon spheres and improve Li^+ storage capacity, we use the nitrogen-doping to improve electrochemical performance of carbon spheres that have the concentric microstructure. Nitrogen doping is an effective method to improve electrochemical performance for a carbon-based electrode and it can increase electrode/electrolyte wettability[37] and electronic conductivity.[37,38] In addition, it also can enhance the Li^+ storage capacity[25,37] and the total capacitance through the pseudocapacitance effects for supercapacitors.[39−41] Recently, diverse research has been performed for nitrogen-doped carbon materials and most studies only concerned synthesis method or the improved electrochemical performance. In general, nitrogen content and type of nitrogen functionalities are not easily controlled, which caused much more difficulties in studying the effect of nitrogen functionalities on improving electrochemical performance. So, it is necessary to investigate the evolution of nitrogen functionalities in carbon materials first to understand the characteristics of nitrogen functionalities.

In this paper, to satisfy both large-scale production and good electrochemical performance, a new, simple, safe and ecologically acceptable method, injecting pyrolysis, was introduced to prepare nitrogen-doped carbon spheres (NDCS). We propose a model for the formation mechanism of NDCS on the basis of the observation of samples that pyrolyzed with different temperature and injecting rate. According to the XPS analysis of NDCS, we describe the evolution of nitrogen functionalities in NDCS. The lithium storage properties of NDCS were also investigated.

MATERIALS AND METHODS

Synthesis of NDCS. A schematic of the injecting pyrolysis system is shown in Figure 1; the synthesis of NDCS was carried out by injecting pyridine droplets directly into a high temperature vertical quartz tube that was placed in a temperature programmable furnace. A quartz crucible was located inside the quartz tube in the constant temperature zone of the furnace. The pyrolysis was under a nitrogen atmosphere and the pyrolysis temperature was 900−1100 °C. According to the pyrolysis temperature and injecting rate (174.6 μm min^{-1}, ca. 24 s per droplet), products are denoted as PYD900, PYD1000 and PYD1100. The desired injecting rate was controlled by an injection pump (TJ-3A/W0109-1B, Baoding Longer Precision Pump Co., Ltd.) with a 2.5 mL syringe. It resulted in a sooty deposition inside the quartz crucible and on the inner wall of the quartz tube. After the furnace was cooled to room temperature, the cotton-like soot that was in the quartz crucible was collected.

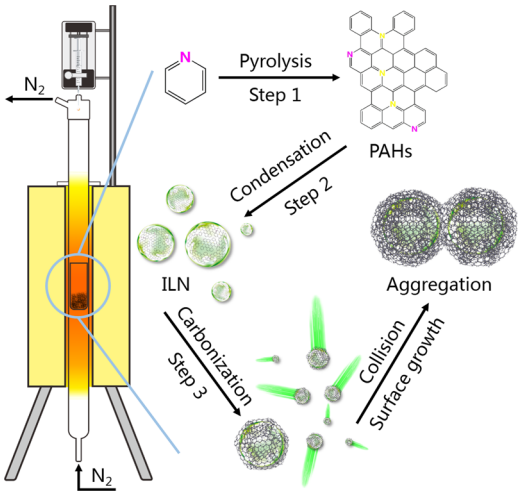

Figure 1. Schematic diagram of the injecting pyrolysis system and the formation mechanism of NDCS.

Characterizations. The NDCS were characterized by scanning electron microscopy (SEM, ZEISS SUPRATM field emission microscope), transmission electron microscopy (TEM, Hitachi H-800), high-resolution transmission electron microscopy (HRTEM, JEOL-2100), X-ray diffraction (XRD, Rigaku D/max-2500B2+/PCX system) using Cu Kα radiation (λ = 1.5406 Å) over the range of 5−90°(2θ) and X-ray photoelectron spectroscopy (XPS, Thermo Electron Corporation ESCALAB 250 XPS spectrometer with monochromatic Al K X-ray sources of 30 eV pass energy in 0.5 eV step over an area of 650 μm × 650 μm and charging correction with reference to C 1s at 285.0 eV). Raman spectra were collected on Renishaw inVia Reflex using 514 nm laser excitation to compare the graphitizaion degree (ratio of D and G band of the carbon) of these samples. Nitrogen adsorption−desorption measurements were performed at −196 °C on a Micromeritics ASAP2020. The samples were degassed at 300 °C for 6 h under a vacuum in the degas port of the analyzer before sorption measurement and specific surface areas (SSA) were estimated according to the Brunauer−Emmett−Teller (BET) model.

Electrochemical Measurements. The electrochemical measurements were carried out by using 2032 coin-type cells with a pure lithium sheet as the counter electrode. The working electrode was prepared by mixing the NDCS powder, poly(vinylidene fifluoride) (PVDF), acetylene black at a weight ratio of 8:1:1, and *N*-methylpyrrolidineone (NMP) was added to form a slurry for spreading the composites onto foam nickel. Then the working electrodes were dried under vacuum at 80 °C for 4 h and 120 °C for 12 h. The electrolyte was 1 M $LiPF_6$ in a 1:1 (volume) mixture of ethylene carbonate and dimethyl carbonate. The cells were assembled in an argon-filled glovebox with concentrations of moisture and oxygen below 1 ppm. The galvanostatically charge−discharge cycles of the cells were measured between 0.01 and 2.50 V versus Li/Li^+ at various current densities by a LAND CT2001 battery tester.

RESULTS AND DISCUSSION

In the pyrolysis experiment, we used pyridine as the precursor and in order to ensure that every pyridine droplet was pyrolyzed completely, the present work first had 174.6 μm min^{-1} (ca. 24 s per droplet) as the injecting rate. It is particularly worth nothing that carbon precursors are not limited to pyridine, and any liquid carbon precursor could be used, such as aromatic heavy oil and coal tar. Therefore, this makes our method much more practical. Figure 2 shows the morphologies of the as-prepared NDCS. SEM images with different magnifications show that the samples consist of almost entire carbon spheres but are severely aggregated. According to Figure 2b, the surfaces of the PYD900 have many little hemispheres on them, and the TEM image in Figure 2d clearly verifies that the small hemispheres are on the outer surface of the aggregated carbon spheres. From Figure 2e,f and Figure 2i,j, PYD1000 and PYD1100 have relatively smooth surfaces. The observation of the broken sphere shown in Figure 2c,g,k and TEM images indicate that these carbon spheres with concentric structures were solid rather than hollow, and this result is similar to that of the previous report.[1] Figure 3b,c shows

DOI: 10.1021/acssuschemeng.5b00359
ACS Sustainable Chem. Eng. 2015, 3, 1786−1793

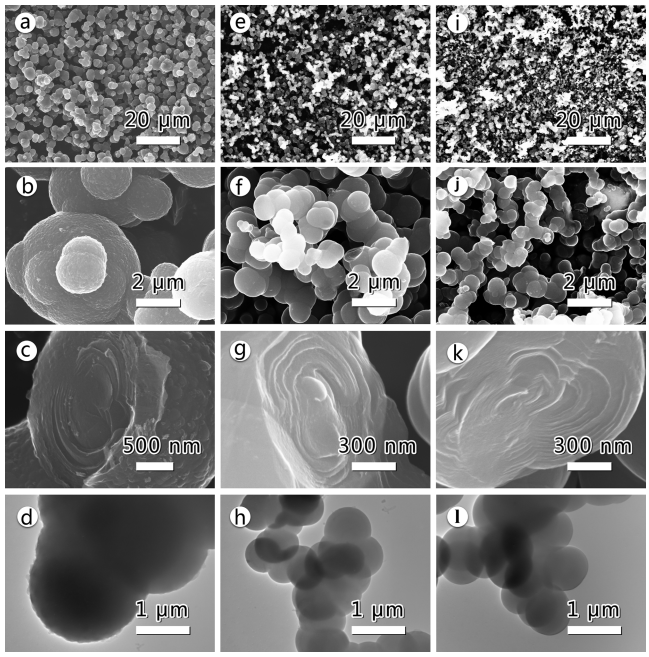

Figure 2. SEM images (a, e and i at low magnification; b, c, f, g, j and k at high magnification) and TEM images (d, h and l) of NDCS from PYD900 (a–d), PYD1000 (e–h) and PYD1100 (i–l), respectively.

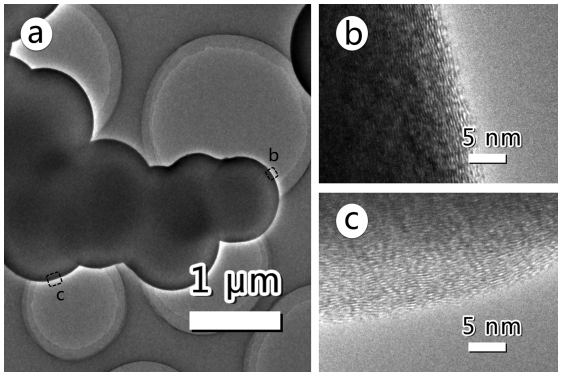

Figure 3. HRTEM images of PYD1000.

HRTEM images at the edge of PYD1000 that indicate that PYD1000 consists of concentric incompletely closed graphitic shells. Obviously, with the pyrolysis temperature increasing, the average diameter of NDCSs was gradually reduced from 2.68 to 1.05 μm. This result is different from an earlier report that the diameters of carbon spheres were not significantly affected with fixed feed times and pyrolysis temperatures between 900 and 1200 °C.[1] Simultaneously, our results also confirm the fact that a catalyst is not essential for the growth of carbon spheres.[1,20]

The BET specific surface areas are measured to be 3.0 $m^2\ g^{-1}$ for PYD1000 and 4.2 $m^2\ g^{-1}$ for PYD1100. But the SSA of PYD900 is too low to measure (maybe below 1 $m^2\ g^{-1}$). These results are consistent with SEM and TEM images, which indicates that NDCS have almost no porous structure.

The carbonization of pyridine in gaseous phase inspired us to associate the formation mechanism of NDCS with carbon black. As shown in Figure 1, we assume the formation mechanism of NDCS is mainly made up of three steps. First step, pyridine molecules are pyrolyzed to aliphatic species[42] then transformed into polyaromatic hydrocarbons (PAHs) by a gas phase reaction. Second step, as the gas phase reaction continues, the partial pressure of PAHs increases until the supersaturation is high enough to induce condensation of PAHs into the initial liquid nucleus (ILN). This process that is so-called nuclei inception[43] in formation of carbon black generates the initial nucleus. In this step, according to Lahaye's results,[44,45] the number of ILN depends only on the supersaturation and temperature, and the number of nucleus increases with temperature. The last step, the ILN are pyrolyzed into an initial solid particle that are wrapped by some graphene layers. At inception, a large number of initial solid particles are collided to produce aggregates. After a long time for surface growth of the aggregates, the aggregated carbon spheres are produced finally until the carbon source is consumed. So, when the carbon source is supplied, the higher temperature in step 2 generates much more initial nuclei that grow into relative small carbon spheres without adding an additional carbon source in the surface growth. This mechanism indicates why the size of NDCS gradually decreases with increasing pyrolysis temperature. On the other hand, the number of ILN is almost the same whether a larger droplet or a small droplet of pyridine is injected into the pyrolysis system at same temperature. But a larger droplet can provide more carbon source for surface growth than a small droplet. In other words, a larger droplet facilitates to produce big carbon spheres due to the sufficient supply of carbon source in surface growth. Oppositely, a small droplet will lead to reduction in size of carbon spheres.[1,20,27]

In step 2, the formation of ILN leads to eliminate supersaturation and thus the formation of additional ILN becomes impossible. If we add carbon source to the pyrolysis system after the formation of ILN and before the end of surface growth, the partial pressure of PAHs could increase again due to the new generation of PAHs, thus the second formation of ILN becomes possible. According to our assumption, the earlier the ILN are formed, the bigger the carbon spheres are generated due to the relative long time for surface growth. Conversely, the later the ILN are formed, the smaller the carbon spheres are generated too. For the purpose of verifing whether our assumption is reasonable, some another pyrolysis experiments were done with improved injecting rates. According to Figure 4, the diameter of most carbon spheres gets smaller and some of them turn bigger when the injecting rate is increased from 174.6 to 2.167 μm min^{-1} (174.6 μm min^{-1} for PYD1000, 722.3 μm min^{-1} for PYD1000-2 and 2.167 μm min^{-1} for PYD1000-3). This trend of variation proves the rationality of our assumption. Therefore, according to the formation mechanism of NDCS, the morphology of NDCS could be easily controlled by the pyrolysis temperature and injecting rate, which are beneficial and practical for large-scale producing high-performance anode material in power Li-ion batteries.

XRD and Raman spectroscopy were used to characterize further the graphitization degrees of NDCS. Figure 5a shows the XRD patterns of samples. Two obvious broadening diffraction peaks at $2\theta \approx 25.6°$ and 43°, which correspond to the (002) and (100) planes of carbon materials and indicate that they are amorphous carbons with low graphitization degree. As the temperature is increased, the (002) peak becomes narrower and the intensity increases, implying the enhancement of graphitization degree of NDCS with pyrolysis temperature. Raman spectroscopy for NDCS are shown in Figure 5b, which display a typical D band (appear at 1360 cm^{-1}) and G band (appear at 1585 cm^{-1}).[46] The D band

DOI: 10.1021/acssuschemeng.5b00359
ACS Sustainable Chem. Eng. 2015, 3, 1786–1793

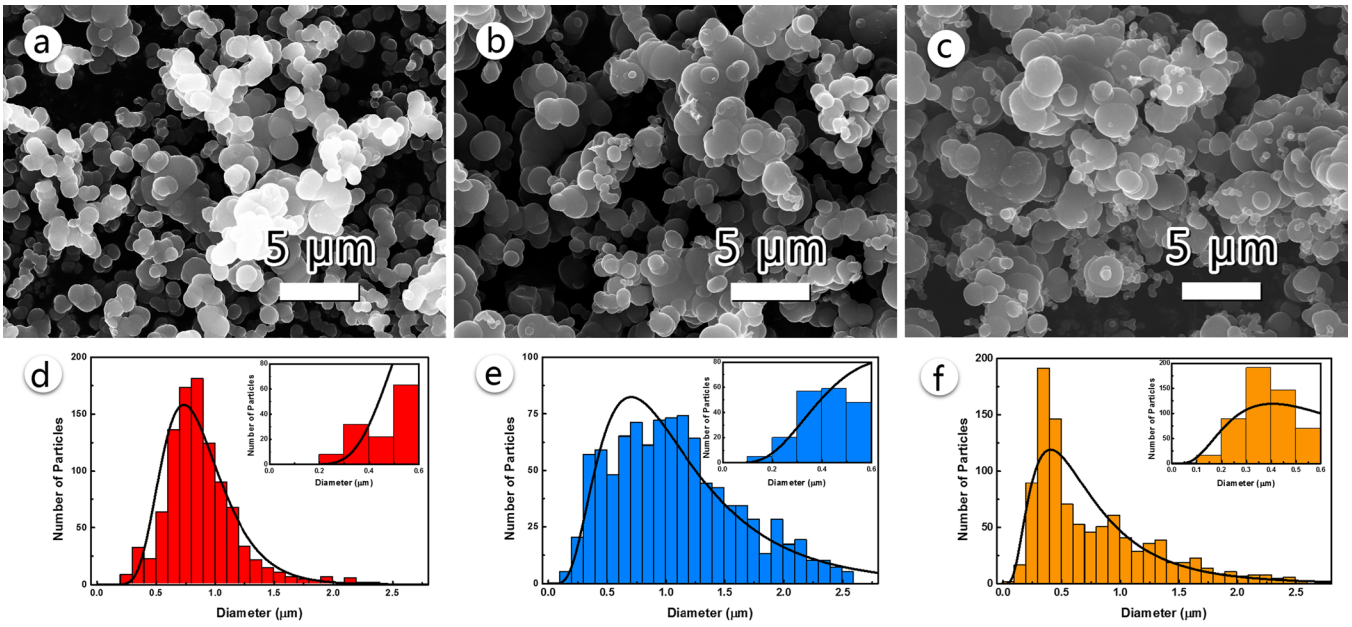

Figure 4. SEM images (a, b and c) and histograms of diameter distribution (d, e and f) from SEM data based on 1000 carbon spheres (manually determined) of NDCS for PYD1000 (a, d), PYD1000-2 (b, e) and PYD1000-3 (c, f), respectively.

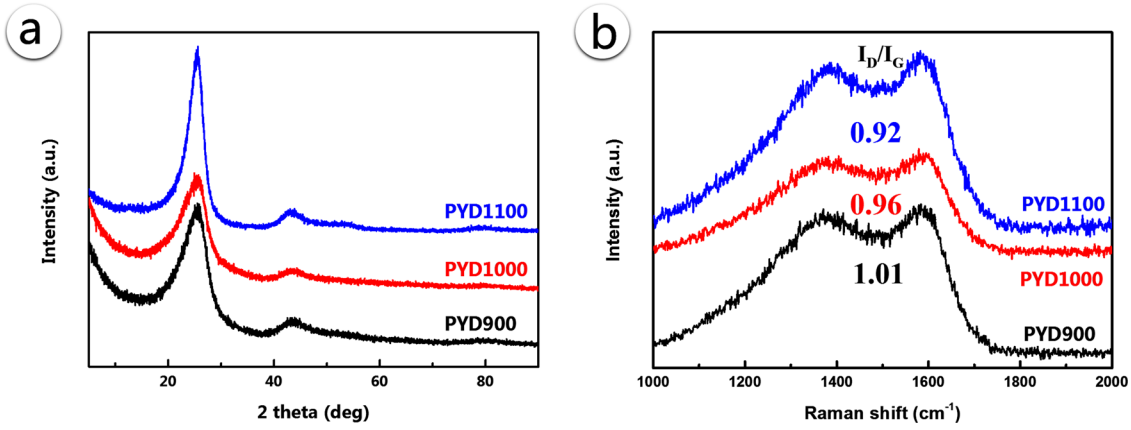

Figure 5. XRD patterns (a) and Raman spectra (b) of NDCS.

corresponds to the disordered and imperfect structures of the carbon material, whereas the G band represents the ordered carbon structure. The decreased I_D/I_G intensity ratio from PYD900 to PYD1100 indicated the enhancement of graphitization degree of NDCS, which corresponds to the results of XRD.

XPS spectra and elemental contents of pyrolysis products are shown in Figure 6 and Table 1, respectively. The weak oxygen content almost certainly is caused by the existence of small quantities of O_2 in the pyrolysis system and adsorbing H_2O by the surface of NDCS. XPS analysis is employed to identify the chemical states of nitrogen in the NDCS. As shown in Figure 6, the N 1s spectrum of NDCS recognized four types of nitrogen: pyridinic-N (N-6, 398.5 ± 0.2 eV), pyrrolic-N (N-5, 400.5 ± 0.2 eV), quaternary-N (N-Q, 402.9 ± 0.2 eV) and pyridine-N-oxide (N-oxide, 403 ± 0.2 eV).[47,48] N-6 and N-5 were formed predominately through substituting a carbon atom by N on edges or defect sites in the plane because such carbon atoms are much more chemically active than those within the plane of perfect graphene.[37] N-Q, i.e., nitrogen atom replaced carbon atom in the graphene plane and bonded to three carbon atoms.[49] According to Table 1, the nitrogen contents of PYD900 is 3.99 at. %, which is similar to that of PYD1000 (3.80 at. %), but the nitrogen content of PYD1100 decreases to 2.86 at. %. Obviously, with the pyrolysis temperature increasing, the nitrogen content of NDCS decreases gradually. This result is in agreement with those of other reports[39,40,48] which may be due to C−N bonds breaking seriously in high temperature heat treatment (above 1000 °C). The N 1s spectrum of PYD900 consists of N-5 (20.90%), N-6 (23.80%), N-Q (50.29%) and N-oxide (5.01%). However, when the pyrolysis temperature was elevated to 1000 °C, 41% of the N-5 peak disappeared and both N-6 and N-Q increased. When heated to 1100 °C, the N-5 peak disappears completely, which proved N-5 functionalities could stable up to 1000 °C and N-6 decrease to 18.91%, but only N-Q increase to 78.49%. The decrease of N-5 peak at high temperatures is similar to earlier reports on thermal treatment of nitrogen containing carbon nanotubes[48] and chars.[50] But the N-5 in NDCS complete disappearing occurs at high temperature than in the carbon nanotubes and chars that show a rather low thermal stability of N-5 functionalities.

DOI: 10.1021/acssuschemeng.5b00359
ACS Sustainable Chem. Eng. 2015, 3, 1786−1793

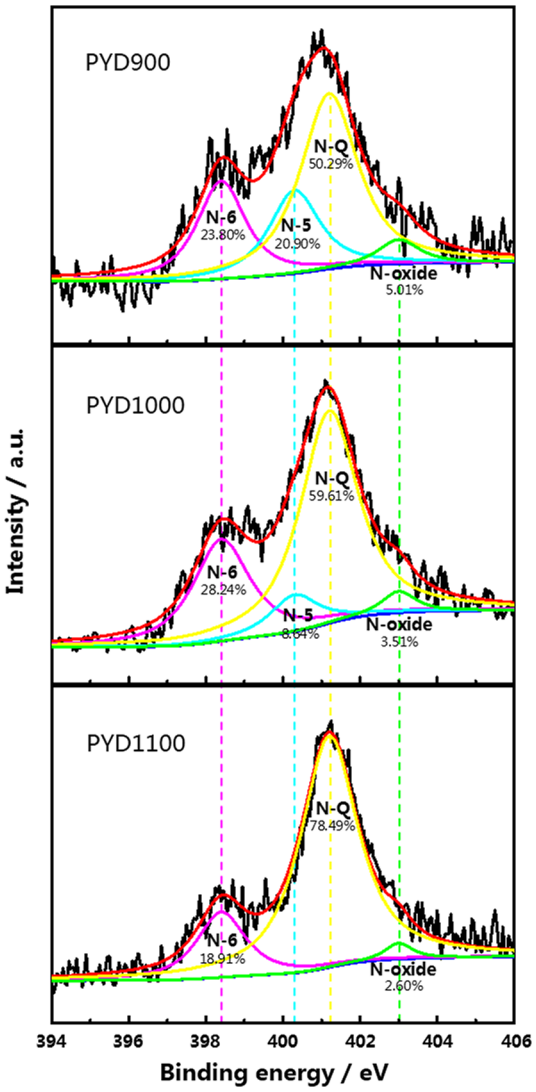

Figure 6. High-resolution N 1s spectra of XPS.

Usually, N-5 functionalities decrease gradually above 600 °C and almost disappear completely below 900 °C;[50] moreover, the total nitrogen content of nitrogen-doping carbon materials prepared by the in situ nitrogen doping decreased seriously at high temperatures (the total nitrogen content was often below ca. 1.5 at. % when pyrolysis temperature was above 900 °C).[39−41] However, the total nitrogen content of PYD1100 prepared by in situ nitrogen doping is still as high as 2.86 at. % and N-5 functionalities in NDCS are still stable in 1000 °C. These results indicate that the microstructure of concentric incompletely closed graphitic shells of NDCS is beneficial to the thermal stability of nitrogen functionalities. Besides, there still is another important observation in our data: the ratio N-Q/N-6 is 2.1 at 900 °C and remains that at 1000 °C, but changed to 4.2 at 1100 °C. When the pyrolysis temperature was increased to 1000 °C from 900 °C, a fast decrease in N-5 and a slow increase both in N-6 and N-Q suggest that N-5 is partly converted to N-6 and N-Q. In this process, it is still unclear whether N-5 is first converted to N-6 and then transformed to N-Q or N-5 is simultaneously converted to both N-6 and N-Q. Finally, when pyrolysis temperature further heated up to 1100 °C from 1000 °C, N-5 disappeared completely and N-6 began to experience a decline. However, the percentage of N-Q increased to the highest value (78.79%). Considering the stability of nitrogen functionalities, this confirms that N-5 inclined to convert into N-Q rather than N-6 in high temperature and N-Q is the most stable nitrogen functionality in N-doped carbon materials.

According to early reports, nitrogen functionalities in various carbon material have different thermal stability, but after severe pyrolysis, all nitrogen is finally presented in 6-membered rings, N-Q, N-6 and N-X.[49,50] In general, nitrogen functionalities in the surface of carbon materials such as nitrogen-doped graphene and carbon nanotubes are easily released in high-temperature heat treatment. Comparing nitrogen-doped graphene with our results, the evolution of nitrogen functionalities in NDCS suggests that the concentric incompletely closed graphitic shells improve the thermal stability of nitrogen functionalities. Evolution of nitrogen functionalities in the formation of NDCS is shown in Figure 7. N-5 could be converted to N-6, N-Q and N-X by "ring expansion"[51] and both N-5 and N-6 could be further converted to N-Q by condensation reactions[50] at relative high temperature. The transformations among nitrogen functionalities are much more complicated and uneasy to distinguish.

Figure 8 illustrates the electrochemical performance of NDCS. The cycling performances of NDCS are depicted in Figure 8a. The Coulombic efficiency of the first cycle are 62.5, 64.2 and 65.8% for PYD900, PYD1000 and PYD1100 electrodes, respectively. This tendency suggests that high heat temperature reduces the surface defects and functional groups. Figure 8c,d shows the galvanostatic charge/discharge voltage profiles at a current density of 50 mA g^{-1}. The voltage plateau at 0.7−0.9 V in the first cycle is due to the formation of the solid electrolyte interface (SEI).[52,53] In the subsequent cycles, the Coulombic efficiency of all samples raises rapidly to 95% in the second cycle and maintains almost as high as 99% for the rest of cycles. As observed, there is almost no capacity fading after the 10th cycle, indicating the excellent cycling performance. PYD900 and PYD1000 exhibit an initial reversible capacity of about 350 mAh g^{-1}. Although PYD1100 has the lowest initial reversible capacity of 320 mAh g^{-1} of the samples, its reversible capacityis still higher than that of the pure carbon spheres (220 mAh g^{-1} at 30 mA g^{-1}),[35] Pureblack graphite (175 mAh g^{-1} at 37 mA g^{-1})[54] and MCMB (294 mAh g^{-1} at 37 mA g^{-1}).[55] The rate performance of NDCS is shown in Figure 8b, highly stable and reversible capacities around 188, 163 and 166 mAh g^{-1} are obtained at 1 A g^{-1} for PYD900, PYD1000

Table 1. Carbon Atomic Percent and Heteroatom Species Content in the NDCS Analysed by XPS

			nitrogen content (atom %)				
sample	carbon content (atom %)	oxygen content (atom %)	total	N-6	N-5	N-Q	N-oxide
PYD900	87.19	8.82	3.99	0.95	0.83	2.01	0.20
PYD1000	90.82	5.38	3.80	1.07	0.33	2.27	0.13
PYD1100	92.63	4.51	2.86	0.54	0	2.25	0.07

DOI: 10.1021/acssuschemeng.5b00359
ACS Sustainable Chem. Eng. 2015, 3, 1786−1793

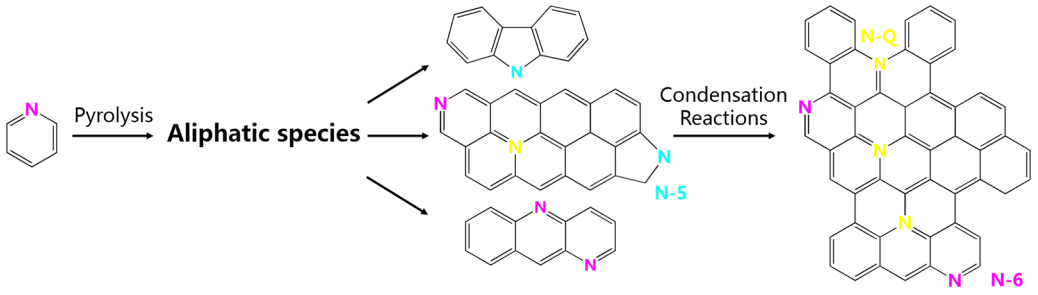

Figure 7. Evolution of nitrogen functionalities in the formation of NDCS during pyrolysis of pyridine.

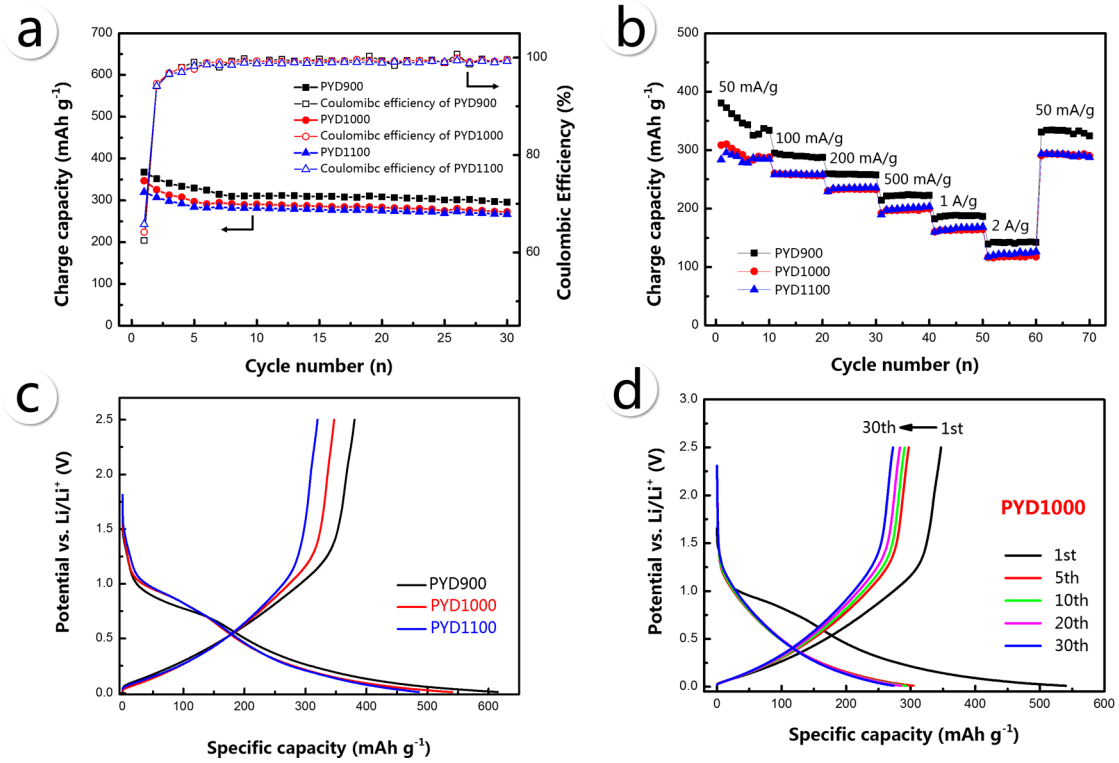

Figure 8. (a) Cycling performance and Coulombic efficiency of NDCS electrodes at current density of 50 mA g^{-1}, (b) rate performance of NDCS at various current densities from 50 mA g^{-1} to 2 A g^{-1}, (c) charge−discharge profiles of NDCS electrodes at first cycle and (d) charge−discharge profiles of PYD1000 at various cycles with current density of 50 mA g^{-1}.

and PYD1100 electrodes, respectively. Obviously, the rate performance of NDCS is superior than that of commercial graphite microspheres (150 mAh g^{-1} at 500 mA g^{-1})[56] and MCMB (no more than 60 mAh g^{-1} at 1.8 A g^{-1}).[54] And this unique rate performance and cycling performance of NDCS should be ascribed to the microstructure of concentric incompletely closed graphitic shells[57] and nitrogen-doping structure.[25,37,38] Nitrogen functionalities can increase the electrode/electrolyte wettability, which promote ion diffusion in the interface between the electrode and electrolyte and the interior of bulk electrode, thus improving the electrochemical performance.[37,58] Furthermore, nitrogen functionalities can promote intercalation of Li-ions by changing the electronic state of carbon atoms.[38,59] But the mechanism of concentric and nitrogen-doping structure favoring stable cycling and high rate performance still need further investigation. Considering its excellent cycling performance and unique synthesis method, NDCS are potential to be used as an anode material for power Li-ion batteries.

CONCLUSIONS

In summary, NDCS with different diameters and nitrogen contents were synthesized by using a one-step facile injecting pyrolysis. The morphology of NDCS could be easily controlled by adjusting pyrolysis temperature and injecting rate. The formation and growth mechanism of NDCS was ascribed to the nuclei inception and surface growth according to the mechanism of gaseous phase carbonization. This mechanism could not only explain the formation of NDCS but also suit for the formation of carbon spheres synthesized by CVD. Moreover, the evolution of nitrogen functionalities in NDCS is useful to help us to understand the transformation of nitrogen functionalities in different microstructures of carbon materials. Considering nitrogen doping is a facile and effective way to enhance the electrochemical property, these make our synthesis method much more practical for large-scale production of high-performance anode materials in power Li-ion batteries.

DOI: 10.1021/acssuschemeng.5b00359
ACS Sustainable Chem. Eng. 2015, 3, 1786−1793

AUTHOR INFORMATION

Corresponding Author

*H. Song. E-mail: songhh@mail.buct.edu.cn. Tel/Fax: +86-010-64434916.

Notes

The authors declare no competing financial interest.

ACKNOWLEDGMENTS

This work was supported by National Natural Science Foundation of China (51272016 and 51272019), and Foundation of Excellent Doctoral Dissertation of Beijing City (YB20121001001).

REFERENCES

(1) Jin, Y. Z.; Gao, C.; Hsu, W. K.; Zhu, Y.; Huczko, A.; Bystrzejewski, M.; Roe, M.; Lee, C. Y.; Acquah, S.; Kroto, H.; Walton, D. R. M. Large-scale synthesis and characterization of carbon spheres prepared by direct pyrolysis of hydrocarbons. *Carbon* **2005**, *43*, 1944−1953.

(2) Kroto, H. W.; Heath, J. R.; O'Brien, S. C.; Curl, R. F.; Smalley, R. E. C60: Buckminsterfullerene. *Nature* **1985**, *318*, 162−163.

(3) Iijima, S. Helical microtubules of graphitic carbon. *Nature* **1991**, *354*, 56−58.

(4) Novoselov, K. S.; Geim, A. K.; Morozov, S. V.; Jiang, D.; Zhang, Y.; Dubonos, S. V.; V, G. I.; A, F. A. Electric Field Effect in Atomically Thin Carbon Films. *Science* **2004**, *306*, 666−669.

(5) Thackeray, M. M.; Wolverton, C.; Isaacs, E. D. Electrical energy storage for transportation—approaching the limits of, and going beyond, lithium-ion batteries. *Energy Environ. Sci.* **2012**, *5*, 7854.

(6) Sevilla, M.; Mokaya, R. Energy storage applications of activated carbons: supercapacitors and hydrogen storage. *Energy Environ. Sci.* **2014**, *7*, 1250.

(7) Zhou, G. M.; Li, F.; Cheng, H. M. Progress in flexible lithium batteries and future prospects. *Energy Environ. Sci.* **2014**, *7*, 1307.

(8) Wang, H.; Dai, H. Strongly coupled inorganic−nano-carbon hybrid materials for energy storage. *Chem. Soc. Rev.* **2013**, *42*, 3088.

(9) Inagaki, M. Carbon materials Structure, texture and intercalation. *Solid State Ionics* **1996**, *86*, 833−839.

(10) Yu, D. S.; Qian, Q. H.; Wei, L.; Jiang, W. C.; Goh, K. L.; Wei, J.; Zhang, J.; Chen, Y. Emergence of fiber supercapacitors. *Chem. Soc. Rev.* **2015**, *44*, 647−662.

(11) Van Noorden, R. A BETTER BATTERY. *Nature* **2014**, *507*, 26.

(12) Tollefson, J. CHARGING UP THE FUTURE. *Nature* **2008**, *456*, 436.

(13) Zhai, Y.; Dou, Y.; Zhao, D.; Fulvio, P. F.; Mayes, R. T.; Dai, S. Carbon Materials for Chemical Capacitive Energy Storage. *Adv. Mater.* **2011**, *23*, 4828−4850.

(14) Dai, L. M.; Chang, D. W.; Baek, J. B.; Lu, W. Carbon Nanomaterials for Advanced Energy Conversion and Storage. *Small* **2012**, *8*, 1130−1166.

(15) Zhang, L. L.; Zhao, X. S. Carbon-based materials as supercapacitor electrodes. *Chem. Soc. Rev.* **2009**, *38*, 2520.

(16) Li, Y.; Fu, Z. Y.; Su, B. L. Hierarchically Structured Porous Materials for Energy Conversion and Storage. *Adv. Funct. Mater.* **2012**, *22*, 4634−4667.

(17) Simon, P.; Gogotsi, Y. Materials for electrochemical capacitors. *Nat. Mater.* **2008**, *7*, 845−854.

(18) Xin, S.; Guo, Y. G.; Wan, L. J. Nanocarbon Networks for Advanced Rechargeable Lithium Batteries. *Acc. Chem. Res.* **2012**, *45*, 1759−1769.

(19) Serp, P.; Feurer, R.; Kalck, P.; Kihn, Y.; Faria, J. L.; Figueiredo, J. L. A chemical vapour deposition process for the production of carbon nanospheres. *Carbon* **2001**, *39*, 621−626.

(20) Qian, H.; Han, F.; Zhang, B.; Guo, Y.; Yue, J.; Peng, B. Non-catalytic CVD preparation of carbon spheres with a specific size. *Carbon* **2004**, *42*, 761−766.

(21) Wang, P.; Wei, J.; Huang, B.; Qin, X.; Yao, S.; Zhang, Q.; Wang, Z.; Xu, G.; Jing, X. Synthesis and characterization of carbon spheres prepared by chemical vapour deposition. *Mater. Lett.* **2007**, *61*, 4854−4856.

(22) Miao, J.; Hwang, D. W.; Narasimhulu, K. V.; Lin, P.; Chen, Y.; Lin, S.; Hwang, L. Synthesis and properties of carbon nanospheres grown by CVD using Kaolin supported transition metal catalysts. *Carbon* **2004**, *42*, 813−822.

(23) Nieto-Márquez, A.; Espartero, I.; Lazo, J. C.; Romero, A.; Valverde, J. L. Direct synthesis of carbon and nitrogen−carbon nanospheres from aromatic hydrocarbons. *Chem. Eng. J.* **2009**, *153*, 211−216.

(24) Wu, H. C.; Hong, C. T.; Chiu, H. T.; Li, Y. Y. Continuous synthesis of carbon spheres by a non-catalyst vertical chemical vapor deposition. *Diamond Relat. Mater.* **2009**, *18*, 601−605.

(25) Wang, Y.; Su, F.; Wood, C. D.; Lee, J. Y.; Zhao, X. S. Preparation and Characterization of Carbon Nanospheres as Anode Materials in Lithium-Ion Secondary Batteries. *Ind. Eng. Chem. Res.* **2008**, *47*, 2294−2300.

(26) Peer, M.; Qajar, A.; Rajagopalan, R.; Foley, H. C. On the effects of emulsion polymerization of furfuryl alcohol on the formation of carbon spheres and other structures derived by pyrolysis of polyfurfuryl alcohol. *Carbon* **2013**, *51*, 85−93.

(27) Zhou, X.; Yang, Z.; Nie, H.; Yao, Z.; Zhang, L.; Huang, S. Catalyst-free growth of large scale nitrogen-doped carbon spheres as efficient electrocatalysts for oxygen reduction in alkaline medium. *J. Power Sources* **2011**, *196*, 9970−9974.

(28) Ko, Y. N.; Park, S. B.; Kang, Y. C. Design and Fabrication of New Nanostructured SnO2 -Carbon Composite Microspheres for Fast and Stable Lithium Storage Performance. *Small* **2014**, *10*, 3240−3245.

(29) Wang, X.; Liu, J.; Xu, W. One-step hydrothermal preparation of amino-functionalized carbon spheres at low temperature and their enhanced adsorption performance towards Cr(VI) for water purification. *Colloids Surf., A* **2012**, *415*, 288−294.

(30) Wang, Q.; Li, H.; Chen, L.; Huang, X. Novel spherical microporous carbon as anode material for Li-ion batteries. *Solid State Ionics* **2002**, *152*, 43−50.

(31) Sevilla, M.; Fuertes, A. B. The production of carbon materials by hydrothermal carbonization of cellulose. *Carbon* **2009**, *47*, 2281−2289.

(32) Pol, V. G.; Motiei, M.; Gedanken, A.; Calderon-Moreno, J.; Yoshimura, M. Carbon spherules: synthesis, properties and mechanistic elucidation. *Carbon* **2004**, *42*, 111−116.

(33) Pol, V. G.; Pol, S. V.; Calderon Moreno, J. M.; Gedanken, A. High yield one-step synthesis of carbon spheres produced by dissociating individual hydrocarbons at their autogenic pressure at low temperatures. *Carbon* **2006**, *44*, 3285−3292.

(34) Inagaki, M. Discussion of the formation of nanometric texture in spherical carbon bodies. *Carbon* **1997**, *35*, 711−713.

(35) Jin, Y. Z.; Kim, Y. J.; Gao, C.; Zhu, Y. Q.; Huczko, A.; Endo, M.; Kroto, H. W. High temperature annealing effects on carbon spheres and their applications as anode materials in Li-ion secondary battery. *Carbon* **2006**, *44*, 724−729.

(36) Zaghib, K.; Brochu, F.; Guerfi, A.; Kinoshita, K. Effect of particle size on lithium intercalation rates in natural graphite. *J. Power Sources* **2001**, *103*, 140−146.

(37) Wu, Z. S.; Ren, W. C.; Xu, L.; Li, F.; Cheng, H. M. Doped Graphene Sheets As Anode Materials with Superhigh Rate and Large Capacity for Lithium Ion Batteries. *ACS Nano* **2011**, *5*, 5463−5471.

(38) Bulusheva, L. G.; Okotrub, A. V.; Kurenya, A. G.; Zhang, H.; Zhang, H.; Chen, X.; Song, H. Electrochemical properties of nitrogen-doped carbon nanotube anode in Li-ion batteries. *Carbon* **2011**, *49*, 4013−4023.

(39) Xu, B.; Duan, H.; Chu, M.; Cao, G. P.; Yang, Y. S. Facile synthesis of nitrogen-doped porous carbon for supercapacitors. *J. Mater. Chem. A* **2013**, *1*, 4565.

(40) Xu, B.; Hou, S.; Cao, G.; Wu, F.; Yang, Y. Sustainable nitrogen-doped porous carbon with high surface areas prepared from gelatin for supercapacitors. *J. Mater. Chem.* **2012**, *22*, 19088−19093.

DOI: 10.1021/acssuschemeng.5b00359
ACS Sustainable Chem. Eng. 2015, 3, 1786−1793

(41) Xu, B.; Zheng, D. F.; Jia, M. Q.; Cao, G. P.; Yang, Y. S. Nitrogen-doped porous carbon simply prepared by pyrolyzing a nitrogen-containing organic salt for supercapacitors. *Electrochim. Acta* **2013**, *98*, 176−182.
(42) Hong, X.; Zhang, T.; Zhang, L.; Qi, F. Identification of Intermediates in Pyridine Pyrolysis with Molecular-beam Mass Spectrometry and Tunable Synchrotron VUV Photoionization. *Chin. J. Chem. Phys.* **2009**, *22*, 204−209.
(43) Lahaye, J.; Ehrburger-Dolle, F. Mechanisms of carbon black formation. Correlation with the morphology of aggregates. *Carbon* **1994**, *32*, 1319−1324.
(44) Lahaye, J.; Prado, G.; Donnet, J. B. Nucleation and growth of carbon black particles during thermal decomposition of benzene. *Carbon* **1974**, *12*, 27−35.
(45) Lahaye, J. Mechanisms of soot formation. *Polym. Degrad. Stab.* **1990**, *30*, 111−121.
(46) Wang, Y.; Alsmeyer, D. C.; McCreery, R. L. Raman spectroscopy of carbon materials: structural basis of observed spectra. *Chem. Mater.* **1990**, *2*, 557−563.
(47) Raymundo-Piñero, E.; Cazorla-Amorós, D.; Linares-Solano, A. The role of different nitrogen functional groups on the removal of SO2 from flue gases by N-doped activated carbon powders and fibres. *Carbon* **2003**, *41*, 1925−1932.
(48) Sharifi, T.; Hu, G.; Jia, X.; Wågberg, T. Formation of Active Sites for Oxygen Reduction Reactions by Transformation of Nitrogen Functionalities in Nitrogen-Doped Carbon Nanotubes. *ACS Nano* **2012**, *6*, 8904−8912.
(49) Li, X.; Wang, H.; Robinson, J. T.; Sanchez, H.; Diankov, G.; Dai, H. Simultaneous Nitrogen Doping and Reduction of Graphene Oxide. *J. Am. Chem. Soc.* **2009**, *131*, 15939−15944.
(50) Pels, J. R.; Kapteijn, F.; Moulijn, J. A.; Zhu, Q.; Thomas, K. M. Evolution of nitrogen functionalities in carbonaceous materials during pyrolysis. *Carbon* **1995**, *33*, 1641−1653.
(51) Jacobson, I. A.; Jensen, H. B. THERMAL REACTIONS OF ORGANIC NITROGEN COMPOUNDS. II. 1-n-BUTYLPYRROLE. *J. Phys. Chem.* **1962**, *66*, 1245−1247.
(52) Flandrois, S.; Simon, B. Carbon materials for lithium-ion rechargeable batteries. *Carbon* **1999**, *37*, 165−180.
(53) Kim, J. S.; Park, Y. T. Characteristics of surface films formed at a mesocarbon microbead electrode in a Li-ion battery. *J. Power Sources* **2000**, *91*, 172−176.
(54) Arrebola, J. C.; Caballero, A.; Hernán, L.; Morales, J. Graphitized Carbons of Variable Morphology and Crystallinity: A Comparative Study of Their Performance in Lithium Cells. *J. Electrochem. Soc.* **2009**, *156*, A986−A992.
(55) Ahn, S.; Kim, Y.; Kim, K. J.; Kim, T. H.; Lee, H.; Kim, M. H. Development of high capacity, high rate lithium ion batteries utilizing metal fiber conductive additives. *J. Power Sources* **1999**, *81*, 896−901.
(56) Yu, J.; Zhan, H. H.; Wang, Y. H.; Zhang, Z.; Chen, H.; Li, H.; Zhong, Z. Y.; Su, F. Graphite microspheres decorated with Si particles derived from waste solid of organosilane industry as high capacity anodes for Li-ion batteries. *J. Power Sources* **2013**, *228*, 112−119.
(57) Wang, H.; Abe, T.; Maruyama, S.; Iriyama, Y.; Ogumi, Z.; Yoshikawa, K. Graphitized Carbon Nanobeads with an Onion Texture as a Lithium-Ion Battery Negative Electrode for High-Rate Use. *Adv. Mater.* **2005**, *17*, 2857−2860.
(58) Andersson, A. M.; Abraham, D. P.; Haasch, R.; MacLaren, S.; Liu, J.; Amine, K. Surface Characterization of Electrodes from High Power Lithium-Ion Batteries. *J. Electrochem. Soc.* **2002**, *149*, A1358.
(59) Li, Y. F.; Zhou, Z.; Wang, L. B. CN_x nanotubes with pyridinelike structures: p-type semiconductors and Li storage materials. *J. Chem. Phys.* **2008**, *129*, 104703.

DOI: 10.1021/acssuschemeng.5b00359
ACS Sustainable Chem. Eng. 2015, 3, 1786−1793